Loop VIII/IX of the Na^+-Citrate Transporter CitS of *Klebsiella pneumoniae* Folds into an Amphipathic Surface Helix†

Iwona Sobczak and Juke S. Lolkema*

Molecular Microbiology, Groningen Biomolecular Sciences and Biotechnology Institute, University of Groningen, Haren, The Netherlands

Received October 20, 2004; Revised Manuscript Received February 9, 2005

ABSTRACT: The sodium ion-dependent citrate transporter CitS of *Klebsiella pneumoniae* is a member of the 2-hydroxycarboxylate transporter (2HCT) family whose members transport divalent citrate in symport with two sodium ions. Profiles of the hydrophobic moment suggested the presence of an amphipathic helical structure in the cytoplasmic loop between transmembrane segments (TMSs) VIII and IX (the AH loop) in all members of the family. Cysteine-scanning mutagenesis was used to study the secondary structure of the AH loop. We have mutated 20 successive residues into cysteine residues, characterized each of the mutants for its transport activity, and determined the accessibility of the residues. Three of the mutants, G324C, F331C, and F332C, had very low citrate transport activity, and two others, I321C and S333C, exhibited significantly decreased activity after treatment of right-side-out membranes with membrane permeable thiol reagent *N*-ethylmaleimide (NEM), but not with membrane impermeable 4-acetamido-4′-maleimidylstilbene-2,2′-disulfonic acid (AmdiS) and [2-(trimethylammonium)ethyl]methanethiosulfonate (MTSET). No protection against NEM was observed with citrate or sodium ions. Labeling of the cysteine residues in the 20 mutants with the fluorescent probe fluorescein 5-maleimide, in membrane vesicles with an inverted orientation, resulted in a clear periodicity in the accessibility of the residues. Residues expected to be at the hydrophobic face of the putative α-helix were not accessible for the label, whereas those at the hydrophilic face were easily accessed and labeled. Pretreatment of whole cells and inside-out membranes expressing the mutants with the membrane impermeable reagent AmdiS confirmed the cytoplasmic localization of the AH region. It is concluded that the loop between TMSs VIII and IX folds into an amphipathic surface helix.

The sodium-dependent citrate transporter CitS of *Klebsiella pneumoniae* belongs to the 2-hydroxycarboxylate transporter (2HCT)[1] family whose members are secondary transporters exclusively found in bacteria (*1*, *2*). Some of the members are sodium ion symporters (CitS, MaeN of *Bacillus subtilis*) and proton symporters (CimH of *B. subtilis*, MaeP of *Streptococcus bovis*), but others are typical precursor/product exchangers that couple the uptake of the substrate to the excretion of a metabolic end product (CitP of *Leuconostoc mesenteroides*, MleP of *Lactococcus lactis*, CitW of *K. pneumoniae*). A characteristic feature of the substrates of the transporters is a 2-hydroxycarboxylate motif, like in citrate, malate, and lactate (*3*−*8*).

The membrane topology model of the CitS protein reveals 11 transmembrane segments (TMSs) with the N- and C-termini at the cytoplasmic and periplasmic side of the membrane, respectively (*9*−*11*). A long hydrophilic loop located in the cytoplasm separates TMSs I−VI in the N-terminal half from TMSs VII−XI in the C-terminal half of the protein. In addition to the central loop, three other considerably long loops are present; one constitutes a hydrophobic segment between TMS V and VI, termed Vb, which is exported into the periplasm, and two others, termed AH and Xa, are cytoplasmic and located in the C-terminal part of the protein. Recently, loop Xa located between TMSs X and XI (see Figure 1A) was postulated to form a unique pore−loop structure (*12*), a structure also identified in CimH of *B. subtilis* in the 2HCT family (*13*). The pore−loop structure together with TMS XI is believed to form an essential part of the translocation site in the proteins. Two cysteine residues in the Xa region of CitS were shown to be accessible for membrane impermeable reagents from the periplasmic side and the cytoplasmic side of the membrane. Access from the periplasmic side was inhibited by binding of the co-ion Na^+ (*12*, *14*). Moreover, mutation of Cys398 in Xa to Ser reduced the affinity for Na^+ by 1 order of magnitude, and a conserved Arg residue at the interface of Xa and TMS XI was shown to bind the substrate (*13*, *15*).

Studies of insertion of truncated versions of CitS fused to alkaline phosphatase lacking its signal sequence (PhoA fusions) into the *Escherichia coli* membrane showed an interesting phenomenon, which led to speculation about the

† This work was supported by a grant from the Netherlands Organization for Scientific Research (NWO-CW).

* To whom correspondence should be addressed: Molecular Microbiology, University of Groningen, Kerklaan 30, 9751 NN Haren, The Netherlands. Phone: +31 50 363 2155. Fax: +31 50 363 2154. E-mail: j.s.lolkema@biol.rug.nl.

[1] Abbreviations: 2HCT, 2-hydroxycarboxylate transporter; TMS, transmembrane segment; RSO, right-side-out; PMS, phenazine methosulfate; NEM, *N*-ethylmaleimide; AmdiS, 4-acetamido-4′-maleimidylstilbene-2,2′-disulfonic acid; MTSET, [2-(trimethylammonium)ethyl]-methanethiosulfonate bromide.

10.1021/bi047759y CCC: $30.25
Published on Web 03/11/2005

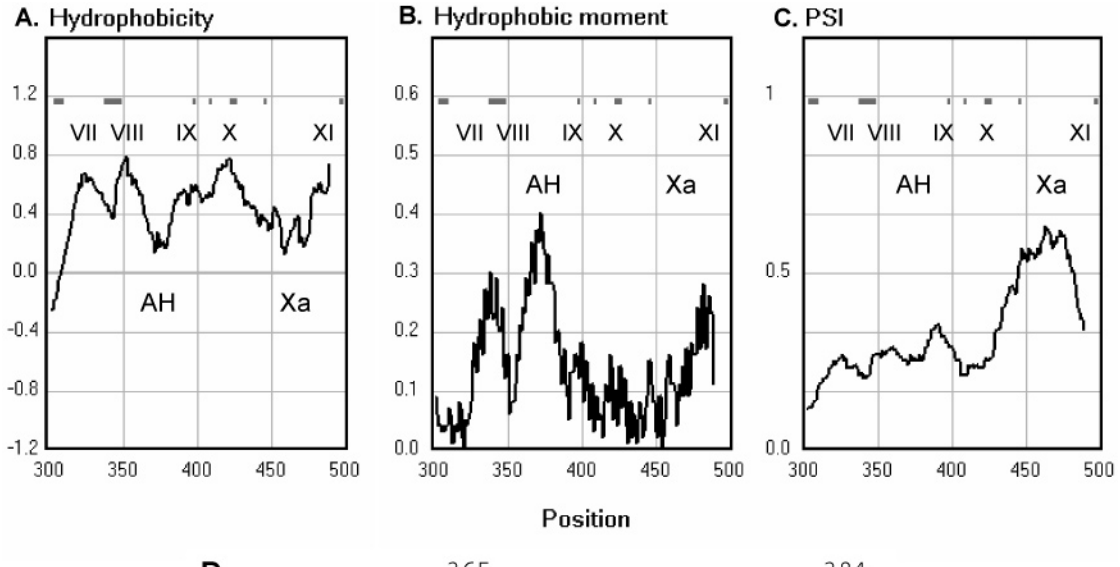

D.

	365		384
CITSkpne	314	SGLCSPEIKAGAKRLSDFFS	333
FN1375fnuc	322	ANLVPDNIKAGAKRMQTFFS	341
CITNcper	313	FNLVPERIRVGAKQVQKFMV	332
BH0400bhal	307	TNMLPKVVLDGASQWYQFVA	326
NP973298tden	300	ANILPKNFENACALWYKFVA	319
MALPsbov	310	LNVVPKETQRGSKQLYKFIS	329
MAENbsub	316	ANILPKKMEEGAYQLYKFIS	335
MAENcvio	309	SKVMPAQMELGAYQMYQFMT	328
CIMHbsub	319	FRLVPASIENGAFGVSRFFS	338
EAK56149eseq	323	ARAVSPPLQEGAFVVYKFFS	342
CITWkpne	322	ANVVSPRLQEGSQMVYKFFR	341
MLEPllac	293	TNTVPKDLEESVVMFNQVIM	312
ZP000379enfa	308	ANLLPEYYEDAAIMFNNLIV	327
CITPlmes	311	FGLLPKYYEDSVIMFGQVIV	330
CITSoyel	240	FNVVSDYYNSCINQASKFVT	259

FIGURE 1: Profile analysis of the C-terminal half of the 2HCT family of secondary transporters. Profiles of the (A) hydrophobicity, (B) hydrophobic moment, and (C) pairwise sequence identity (PSI) were calculated using a window size of 20 residues. The PSI profile gives the fraction of identities at each position in the alignment in an all-against-all comparison averaged over the window. The profiles are based on a multiple-sequence alignment of a set of 15 representative members of the 2HCT family. The hydrophobicity scale was that from ref *25*. The hydrophobic moment profile is based on a periodicity of 100°. Bars in the top parts of the panels represent positions of gaps in any of the sequences in the multiple-sequence alignment. (D) Part of the multiple-sequence alignment showing the AH loop located between TMSs VIII and IX. Numbers in the top line indicate positions in the multiple-sequence alignment. Other numbers refer to the residue numbers of the individual sequences. Abbreviated names of organisms: kpne, *K. pneumoniae*; fnuc, *Fusobacterium nucleatum*; cper, *Clostridium perfringens*; bhal, *Bacillus halodurans*; tden, *Treponema denticola*; sbov, *S. bovis*; bsub, *B. subtilis*; cvio, *Chromobacterium violaceum*; eseq, environmental sequence; llac, *L. lactis*; enfa, *Enterococcus faecalis*; lmes, *Le. mesenteroides*; oyel, *Onion yellows*.

function of loop AH between TMSs VIII and IX. In a CitS molecule truncated at the end of the AH loop, the loop and the preceding TMS VIII were found to reside in the periplasm rather than to have transmembrane (TMS VIII) and cytoplasmic (AH) locations as in the full-length protein. Only when the truncate was extended with downstream TMS IX did TMS VIII insert into the membrane, thereby positioning loop AH in the cytoplasm. Apparently, the presence of TMS IX was both essential and sufficient for proper insertion of both TMSs VIII and IX (*16*). A model for the cotranslational insertion (*17*) of this part of the protein was proposed in which TMS VIII, a highly hydrophobic TMS, would drive the insertion of TMS IX, the least hydrophobic TMS in CitS (*18*). Consequently, the insertion of TMS VIII would be delayed until TMS IX would emerge from the ribosome. It was noted before that the loop between TMSs VIII and IX (the AH loop) would be strongly amphipathic when folded as an α-helix, possibly forming a surface helix (*10*, *11*). Possibly, the amphipathic property of the loop plays a role in the cooperative insertion mechanism of TMSs VIII and IX, for instance, in the delayed insertion of TMS VIII.

Here, we investigate the folding and the role in the transport function of the AH loop by using cysteine-scanning mutagenesis followed by accessibility studies of the Cys residues by thiol specific reagents. The results strongly support the conclusion that in the matured protein the AH loop is folded as an amphipathic α-helix with its hydrophilic side facing the water phase and its hydrophobic side facing the protein.

EXPERIMENTAL PROCEDURES

Bacterial Strains, Growth Conditions, and CitS Constructs. *E. coli* strains DH5α and ECOMUT2 (*19*) were routinely grown in Luria-Bertani broth (LB) at 37 °C under continuous shaking at 150 rpm. When appropriate, the antibiotics ampicillin and chloramphenicol were added at final concentrations of 50 and 30 μg/mL, respectively. All genetic manipulations were carried out in *E. coli* DH5α, while the

CitS protein was expressed in *E. coli* ECOMUT2 harboring plasmid pBADCitS and derivatives. Plasmid pBADCitS is based on vector pBAD24 (Invitrogen) and encodes the wild-type CitS protein with an N-terminal His tag. Expression of the gene is under control of the arabinose promoter (*14*). Expression of CitS was induced by adding 0.1% arabinose when the optical density of the culture measured at 660 nm (OD_{660}) reached a value of 0.6.

Cysteine mutants of CitS were constructed by PCR using the QuickChange Site-Directed Mutagenesis Kit (Stratagene, La Jolla, CA). Plasmid pCSCSS was constructed from plasmid pCCCSS (described in ref *14*) by mutating Cys317 to Ser. Plasmids pCSCSS and pSSSSS encoding Cys-less CitS (*14*) were used as the templates for creating cysteine mutants in loop VIII/IX. All mutants were sequenced (ServiceXS, Leiden, The Netherlands) to confirm the presence of the desired mutations and cloned into the pBAD24 vector as described previously (*14*).

Preparation of Right-Side-Out and Inside-Out Membrane Vesicles. E. coli ECOMUT2 expressing CitS variants were harvested from a 1 L culture by centrifugation at 10000*g* for 10 min at 4 °C. Right-side-out (RSO) membrane vesicles were prepared by the osmotic lysis procedure as described previously (*20*).

Inside-out (ISO) membranes were prepared by washing the cells once with 10 mM Tris-HCl buffer (pH 8), followed by resuspension in 10 mL of 50 mM KP_i buffer (pH 7) containing 2 mM $MgSO_4$ and 10 μg/mL deoxyribonuclease. The suspension was passed once through a French press operated at 13K psi. Cell debris and unbroken cells were removed by centrifugation at 8000 rpm for 10 min at 4 °C in a Beckman SS34 rotor. Membranes were collected by ultracentrifugation for 25 min at 80 000 rpm and 4 °C in a Beckman TLA 100.4 rotor and washed once with 50 mM KP_i (pH 7).

RSO and ISO membranes were resuspended in low-Na^+ 50 mM KP_i (pH 7.0), rapidly frozen, and stored in liquid nitrogen. Membrane protein concentrations were determined by the *DC* Protein Assay Kit (Bio-Rad Laboratories, Hercules, CA).

Immunoblot Analysis. Samples containing 20 μg of total membrane protein were loaded onto a 12.5% sodium dodecyl sulfate−polyacrylamide gel (SDS−PAGE). After electrophoresis, the proteins were transferred to polyvinylidene difluoride (PVDF) membranes (Roche Diagnostic GmbH, Mannheim, Germany) by semi-dry electroblotting. The blots were analyzed using monoclonal antibodies directed against the His tag (Dianova, Hamburg, Germany). Antibodies were visualized using the Western-light chemiluminescence detection kit (Tropix, Bedford, MA). Expression levels were estimated by determining the chemiluminescence intensity of each band using a Lumi-Imager F1 imager (Roche Diagnostic GmbH).

Partial Purification of CitS Derivatives Using Ni−NTA Affinity Chromatography. ISO membranes (4 mg/mL) containing His-tagged CitS derivatives were solubilized in 50 mM KP_i (pH 8), 400 mM NaCl, 20% glycerol, and 1% Triton X-100. The solution was left on ice for 30 min. Undissolved material was removed by ultracentrifugation at 80 000 rpm for 25 min at 4 °C. The supernatant was mixed with Ni^{2+}−NTA resin (100 μL bed volume per 10 mg of protein), equilibrated in 50 mM potassium phosphate (pH 8.0), 600 mM KCl, 10% glycerol, 0.1% Triton X-100, and 10 mM imidazole, and incubated for 1 h at 4 °C while being continuously shaken. After incubation, the resin was pelleted down by pulse centrifugation and the supernatant was removed. The pellet was washed with 10 volumes of equilibration buffer containing 300 mM KCl and 40 mM imidazole. The protein was eluted with 1 bed volume of the same washing buffer but containing 50 mM potassium phosphate (pH 7.0) and 150 mM imidazole, and stored at −20 °C.

Transport Assay in RSO Membranes. Uptake was assessed by the rapid filtration method. RSO membranes were energized using the potassium ascorbate/phenazine methosulfate (PMS) electron donor system (*21*). Membranes were diluted to a final concentration of 0.5 mg/mL in 50 mM KP_i (pH 6.0) containing 70 mM Na^+ unless stated otherwise, in a total volume of 100 μL at 30 °C. Under a constant flow of water-saturated air, and while being magnetically stirred, the mixture was supplemented with 10 mM potassium ascorbate and 100 μM PMS (final concentration), and the proton motive force was allowed to develop for 2 min. Then, [1,5-^{14}C]citrate (114 mCi/mmol, Amersham Pharmacia, Roosendaal, The Netherlands) was added to a final concentration of 4.4 μM. The uptake was stopped by the addition of 2 mL of ice-cold 0.1 M LiCl, followed by immediate filtration over cellulose nitrate filters (pore size of 0.45 μm). The filters were washed once with 2 mL of the 0.1 M LiCl solution and assayed for radioactivity. The background was estimated by adding the radiolabeled substrate to the vesicle suspension after the addition of 2 mL of ice-cold LiCl, immediately followed by filtering. When indicated, experiments were carried out in low-Na^+ KP_i buffer that contains at most 0.005% Na^+, while standard KP_i buffers may contain up to 0.3%.

Treatment of RSO and ISO Membranes with Thiol Reagents. Stock solutions of NEM, MTSET, and AmdiS were prepared freshly in water. RSO membranes at a concentration of 1 mg/mL and ISO membranes at a concentration of 2 mg/mL were treated for the indicated times with the thiol reagents in 50 mM KP_i (pH 7.0) at 20 °C. The treatment was stopped by addition of an equal concentration of DTT in the case of NEM and AmdiS, or reduced glutathione (GSH) in the case of MTSET. The effect of Na^+ on the treatment was determined by adding mixtures of NaCl and KCl that yielded the same concentration of chloride. The effect of citrate on the treatment was measured by adding citrate from a 0.5 M stock solution adjusted to pH 6.0.

After the treatment, RSO membranes were diluted twice into 50 mM KP_i (pH 5.0). If necessary, NaCl and KCl were added to make the Na^+ concentrations equal 70 mM. The resulting suspension was at pH 6 and was immediately used to measure uptake activity. The presence of DTT or GSH did not affect the uptake rate in control experiments. Following the treatment in the presence of citrate, the membranes were washed twice with 50 mM KP_i (pH 6.0) by centrifugation for 20 min in a Beckman Optima TLX ultracentrifuge in a TLA100.2 rotor, to remove citrate. Membranes were resuspended in 50 mM KP_i (pH 6.0) containing 70 mM Na^+ and assayed for uptake activity. The control experiment showed that the washing procedure resulted in a loss of 10−15% of the uptake activity.

After the treatment, ISO membranes were treated with 0.1 mM fluorescein 5-maleimide (FM) for 5 min at 20 °C. The reaction was quenched with 0.5 mM DTT, and after that, CitS derivatives were partially purified using Ni−NTA affinity chromatography as described above. The eluted fraction with a volume of 30 μL was mixed with SDS sample buffer, and 25 μL samples were run on a 12% SDS−PAGE gel. The fluorescence of proteins labeled with FM was visualized on a Lumi-Imager F1 imager (Roche Diagnostic GmbH) by irradiation with UV light using a 520 nm filter. All samples containing FM were kept out of bright light until the gel was exposed. After exposure, the gel was stained with Coomassie Brilliant Blue (CBB) to compare the protein levels of CitS. Quantification was carried out using Lumi-Analyst 3.1 supplied by Roche Diagnostic.

Labeling of Whole Cells with AmdiS. E. coli ECOMUT2 (25 mL culture) cells expressing cysteine mutants or the GltT mutant (see the Results) were washed with 50 mM KP_i buffer (pH 7.0) and resuspended in 1 mL of the same buffer. When indicated, the cell suspension was incubated with 0.25 mM AmdiS for 5 min at 30 °C and the reaction was stopped with DTT (final concentration of 0.5 mM). Subsequently, cells were broken with a Soniprep 150 sonicator operated at an amplitude of 8 μm. Debris was removed by centrifugation at 9000*g* for 10 min. Membranes were collected from the supernatant by centrifugation for 25 min at 80 000 rpm in a Beckman TLA 100.2 rotor at 4 °C and resuspended in low-Na^+ KP_i buffer (pH 7.0). Labeling of membranes with 0.1 mM FM and purification of the CitS derivatives using Ni−NTA affinity chromatography was carried out as described above.

Materials. 2-(Trimethylammonium)ethyl methanethiosulfonate bromide (MTSET) was purchased from Anatrace Inc. NEM was purchased from Sigma-Aldrich BV (Zwijdrecht, The Netherlands). AMdiS and FM were purchased from Molecular Probes Europe BV (Leiden, The Netherlands). Low-Na^+ potassium buffer (KH_2PO_4) was purchased from Merck (E. Merck, Darmstadt, Germany).

RESULTS

Sequence Analysis of Loop VIII/IX of the Members of the 2HCT Family. Figure 1A shows the hydropathy profile of the C-terminal half of the multiple-sequence alignment of 15 typical members of the 2HCT family, including CitS of *K. pneumoniae*. Cytoplasmic loop AH between TMSs VIII and IX shows up as a moderately hydrophobic loop. The profile of the hydrophobic moment with an α-helical periodicity reveals a strong signal around position 370 in loop AH, indicating that when folded as an α-helix the structure would be strongly amphipathic (Figure 1B). The profile averages over the 15 sequences, but inspection of the individual sequences revealed that all sequences show a hydrophobic moment at this position approximately equal in strength (not shown) indicating that the property is conserved throughout the family. The pairwise sequence identity profile (Figure 1C) shows that the sequence of the loop is not particularly well conserved, in contrast to loop Xa that is believed to be part of the translocation site. The low level of sequence identity is also evident from the part of the multiple-sequence alignment representing the AH loop in Figure 1D. In conclusion, while the sequence of loop AH is not well conserved, the amphipathic character of the loop when folded as an α-helix seems to be well conserved in all members of the family.

Cysteine-Scanning Mutagenesis of Loop VIII/IX of CitS. Site-directed mutagenesis was used to substitute each of the residues in loop AH of CitS (top line in Figure 1D) for a cysteine residue. The wild-type CitS protein contains five cysteine residues (indicated as CCCCC), three in cytoplasmic loops in the C-terminal part of the protein and two in the middle of TMSs VII and IX. Mutant CSCSS, in which the three cysteine residues located in the cytoplasmic loops were mutated to serine residues, was used as the parent for the mutants in loop AH. Mutant CSCSS did not react with any of the thiol reagents used in this study (see below). In total, 19 mutants were created. Mutant CCCSS that contains the endogenous Cys317 in loop AH was constructed previously (*14*).

The 20 cysteine mutants in loop AH were tested for their ability to accumulate [1,5-^{14}C]citrate in right-side-out (RSO) membrane vesicles prepared from *E. coli* ECOMUT2 expressing the CitS derivatives in the presence of a proton motive force (pmf) that was generated using the artificial ascorbate/PMS electron donor system (Figure 2A). The expression level of the mutants was estimated by Western blotting using antibodies raised against the His tag present at the N-terminus of the proteins (Figure 2B). The parental mutant CSCSS showed an activity comparable to the wild-type activity (CCCCC). Sixteen of the mutants exhibited an uptake activity in the range of 50−120% of the activity observed for wild-type CitS, while the levels of expression were more or less similar. Two mutants, A325C and K326C, exhibited surprisingly high transport activities of ∼230 and ∼160%, respectively, but their expression level was also higher than average, suggesting that the specific activity was not affected by the mutations. Mutants G324C, F331C, and F332C exhibited very low activity of ≤10%. While for all CitS derivatives, including the wild-type protein, some degradation was observed (lower bands, Figure 2B), mutant G324C clearly showed enhanced degradation, suggesting that for this mutant the lower activity at least in part may be explained by the lower stability of the protein. At any rate, the three mutations significantly reduce the activity of CitS.

Effect of NEM Treatment on Transport Activity. As demonstrated previously (*14*), wild-type CitS was readily inactivated by treatment with the membrane permeable thiol reactive reagent *N*-ethylmaleimide (NEM), while in the presence of the co-ion Na^+, inactivation was essentially completely prevented under the same conditions (Figure 3, black and gray bars, respectively). The protective effect is believed to be due to a conformational change in the protein that occurs upon binding of Na^+ to the Xa region (*12, 14*). It was demonstrated that the two cysteine residues in the Xa loop were responsible for the inactivation which is in line with the insensitivity of the CSCSS mutant to NEM following the same treatment (Figure 3). Eighteen of the 20 mutants in loop AH were insensitive or only marginally affected by the NEM treatment, while two mutants, I321C and S333C, showed a significantly decreased uptake activity (Figure 3, black bars) of less than 50% of untreated membranes. Neither mutant was differently affected in the presence or absence of Na^+, indicating that the conformational change induced by sodium binding is not sensed in

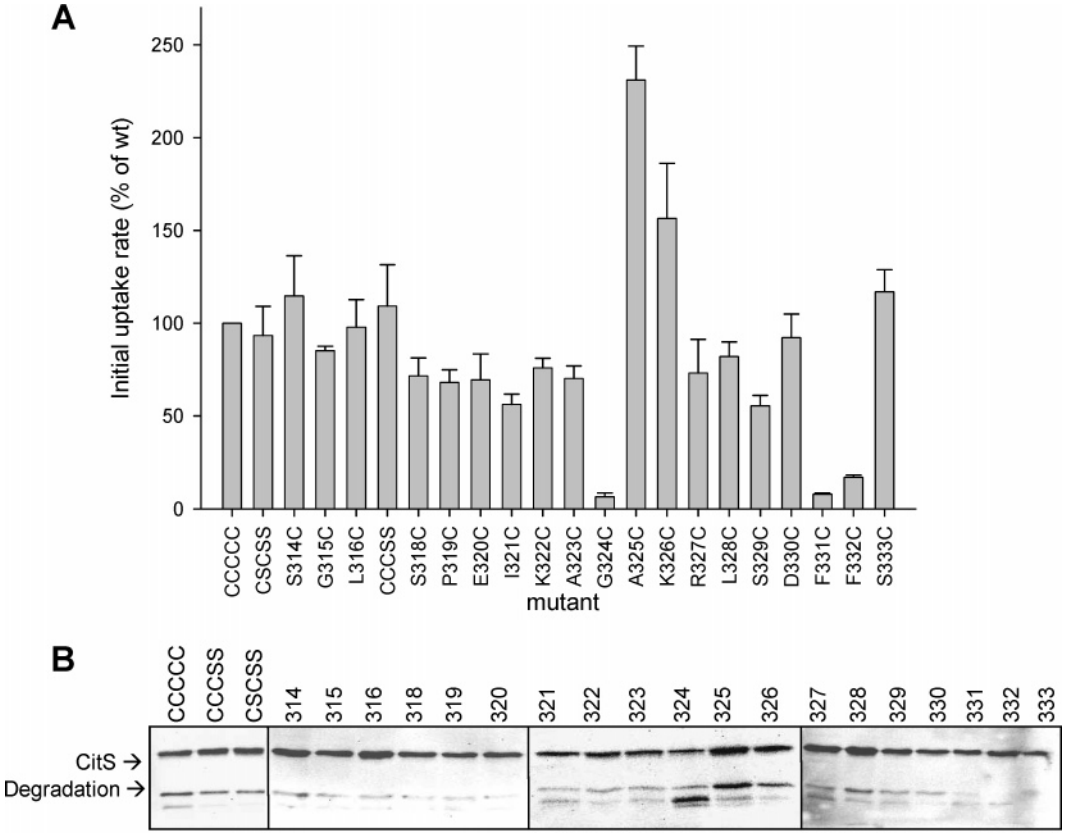

FIGURE 2: Citrate uptake activity of the AH loop cysteine mutants and their expression level. (A) Initial rates of citrate uptake in RSO membranes containing cysteine mutants were expressed as the percentage of the rate measured in membrane vesicles containing wild-type CitS (CCCCC). The bars represent the average and standard deviation obtained from at least three independent measurements. Mutant CCCSS contains the endogenous Cys317. (B) Expression levels of wild-type CitS, the mutant CSCSS, and cysteine mutants in the AH region on a Western blot, stained with antibodies against the His tag. Error bars represent the standard deviations from two or three independent measurements.

the AH loop. To exclude the possibility that the introduction of the cysteine residues at positions 321 and 333 would expose the two cysteine residues in TMSs VII and IX in parental mutant CSCSS, mutants I321C and S333C were constructed in the Cys-less background SSSSS. Inactivation of citrate uptake in membrane vesicles containing these mutants by NEM, in the presence or absence of Na^+, gave similar results as observed with the mutants in the CSCSS background, showing that the effects are due to modification of the cysteine residues at positions 321 and 333 (not shown).

Characteristics of I321C and S333C Mutants. The reactivity of mutants I321C and S333C with NEM was very different. I321C was inactivated slowly but completely with a half-time of ~4 min at a NEM concentration of 2 mM (Figure 4A). S333C was inactivated very quickly with a half-time on the order of seconds under the same conditions, but the maximally obtained inactivation was ~65% (Figure 4B). Increasing the time of inactivation or the NEM concentration did not result in any further loss of activity (not shown).

Because NEM is a membrane permeable reagent, the membrane impermeable thiol reagents AmdiS and MTSET were tested for their ability to inactivate the two CitS mutants in RSO membranes. AmdiS is a maleimide derivative with a bulky negatively charged group, while the methanethiosulfonate derivative MTSET is positively charged and much smaller, of the size of the natural substrate, citrate (*22*). Since the MTS reagent is known to interfere to some extent with the pmf-generating system in the membranes (*14*, *23*), the decrease in the uptake activity by parental mutant CSCSS following the treatment was used as a control (Table 1). Neither AmdiS nor MTSET was able to significantly affect the activity of either mutant I321C or S333C more than observed in the control experiment, which suggests that NEM reaches the cysteine residues from the cytoplasmic side of the membrane.

Previous experiments (*12*) showed that cysteine residues located in the Xa region of the CitS protein could be (partially) protected against modification with thiol reagents after binding of sodium ions or the substrate citrate. No effect on the inactivation by NEM of either I321C or S333C was observed in the presence of Na^+ (Figure 3), citrate, or both substrate and co-ion (not shown).

Accessibility of the Cys Mutants in ISO Membranes. The accessibility of the cysteine residues was studied by treatment of the mutant proteins in ISO membranes with the fluorescent thiol reagent fluorescein maleimide (FM), followed by purification of the proteins using His tag affinity chromatography, SDS−PAGE, and, finally, fluorescence imaging of the gel. The membranes were divided into two aliquots, one of which was pretreated for 10 min with 0.25 mM AmdiS after which both were treated for 5 min with 0.1 mM FM. The mutants were categorized in three groups according to the labeling intensity of the protein from the aliquot that did not receive AmdiS relative to the intensity of the same protein band stained with Coomassie Brilliant Blue (Figure 5A, lanes marked −). Parental mutant CSCSS did not show

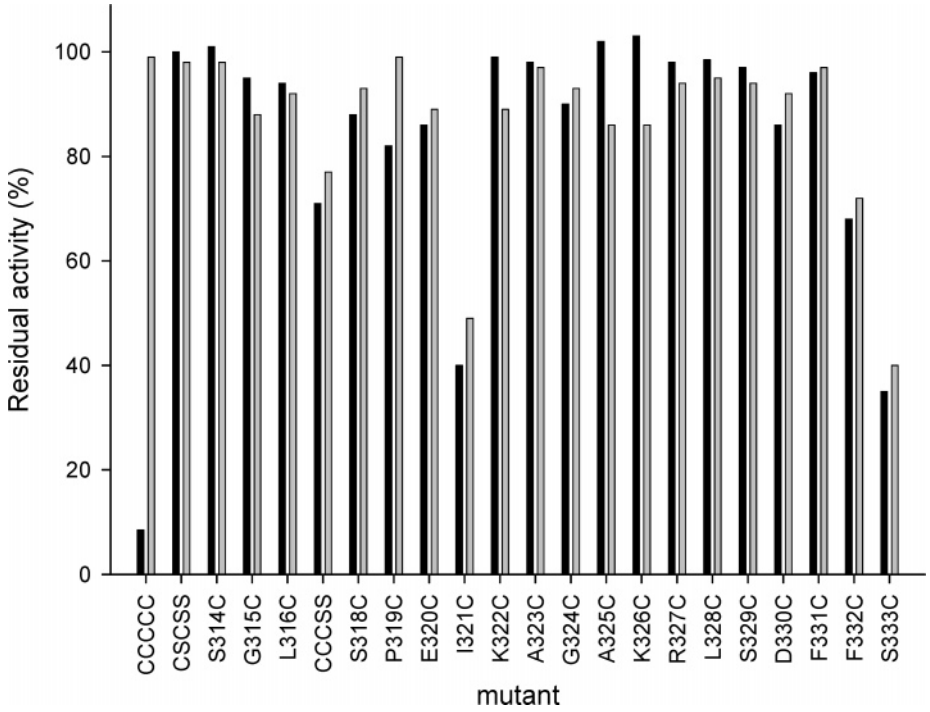

FIGURE 3: Residual activity of citrate uptake in RSO membranes containing the AH cysteine mutants after treatment with 1 mM NEM in the absence (black bars) and presence (gray bars) of 100 mM Na^+ during the treatment. Residual activity represents the initial rate as a percentage of the initial rate catalyzed by untreated membranes. On average, the standard deviation from two or three experiments varied between 5 and 8% of the indicated value.

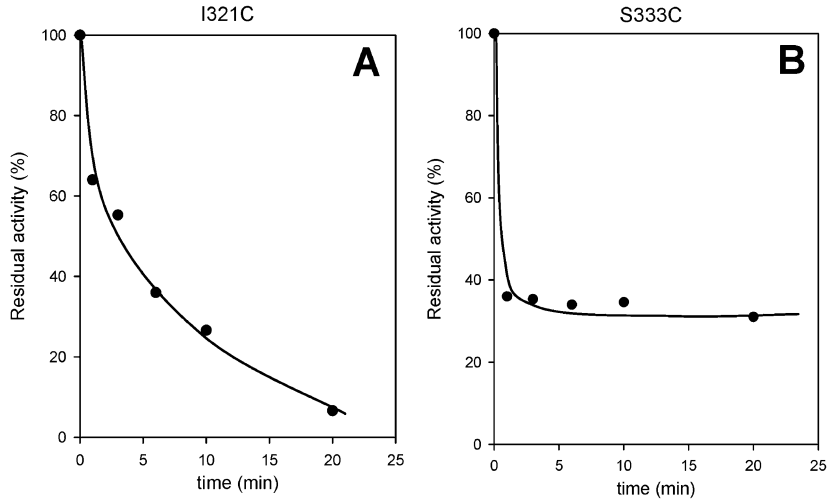

FIGURE 4: Inactivation of mutants I321C (A) and S333C (B) by NEM. Residual activity of the uptake of [1,5-^{14}C]citrate after treatment of RSO membrane vesicles containing CitS mutants I321C (A) and S333C (B) for the indicated time with 2 mM NEM. Residual activity was presented as the percentage of the initial rate catalyzed by untreated membranes. Results are from a typical experiment that was reproduced in triplicate.

any labeling upon treatment with FM (Figure 5B). Similarly, mutants S314C, L316C, C317, I321C, K322C, and L328C were not labeled at all or only very poorly; mutants E320C, G324C, A325C, R327C, S329C, F331C, and F332C were labeled at an intermediate level, and G315C, S318C, P319C, A323C, K326C, D330C, and S333C were labeled strongly. The three categories were indicated on the helical wheel in Figure 6 as filled, hatched, and empty circles, respectively. With few exceptions, residues that were not accessible cluster at the hydrophobic face of the helix while residues that are fully accessible are at the opposite face.

In all cases, labeling of the mutants with FM was prevented by pretreatment with AmdiS, indicating that the positions that were accessible to FM were also accessible to AmdiS in ISO membranes (Figure 5, lanes marked +) which contrasts with the results with mutants I321C and S333C in RSO membranes (Table 1).

Accessibility of the Cys Mutants in Whole Cells. To confirm the cytoplasmic localization of the complete AH region, the accessibility of the cysteine residues in the mutants for membrane impermeable AmdiS was determined in whole cells. Cells expressing mutants G315C, P319C, A323C, K326C, D330C, and S333C, all of which were readily accessible for both AmdiS and FM in ISO membranes, were treated for 10 min with 0.25 mM AmdiS followed by purification of the mutants and labeling with the fluorescent probe FM. The labeling intensity of all six mutants that cover the complete AH region was the same in

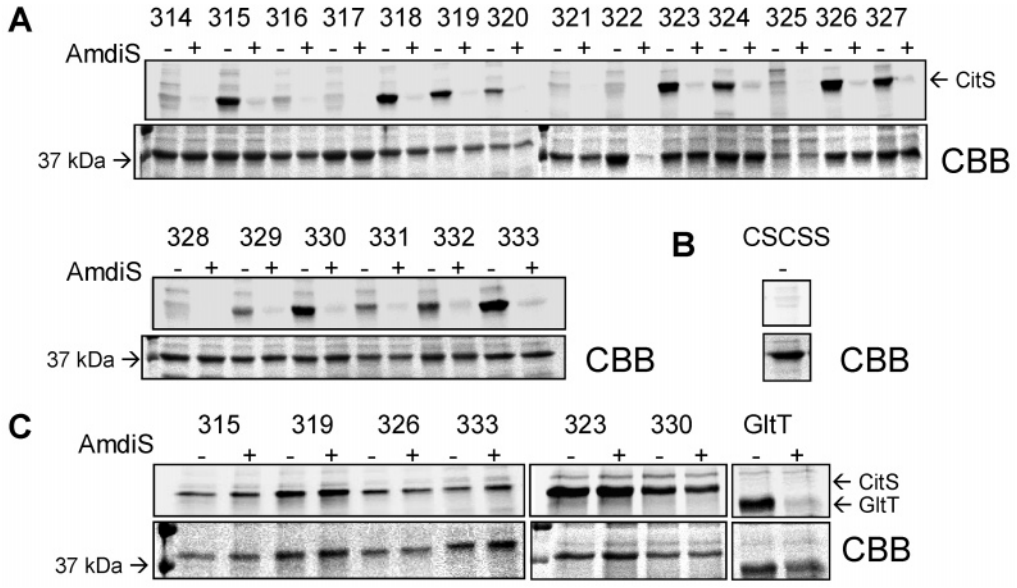

FIGURE 5: Accessibility of cysteine residues in the AH cysteine mutants. (A) ISO membranes containing cysteine mutants were pretreated with (+) or without (−) AmdiS followed by labeling with 0.1 mM fluorescein maleimide (FM) for 5 min. The numbers indicate the position of the cysteine residues in the CitS sequence. Top rows show the fluorescence image of the CitS containing part of the gel and bottom rows (CBB) the same part of the gel after Coomassie Brilliant Blue staining. On the left, the markers are shown (37 kDa). (B) ISO membranes containing mutant CSCSS labeled with FM as described above. (C) Whole cells expressing cysteine mutants of CitS and GltT (control) were pretreated with (+) and without (−) AmdiS followed by preparation of ISO membranes and labeling with 0.1 mM FM for 5 min as described in Experimental Procedures.

Table 1: Inactivation of Cysteine Mutants I321C and S333C with Different Thiol Reagents

		residual activity (%)	
mutant	treatment[a]	CSCSS	CXCSS
I321C	NEM for 10 min	96 ± 3	27 ± 7
	AmdiS for 10 min	91 ± 6	97 ± 7
	MTSET for 10 min	51 ± 5	45 ± 6
S333C	NEM for 1 min	96 ± 7	36 ± 8
	AmdiS for 1 min	91 ± 5	89 ± 6
	MTSET for 1 min	79 ± 5	64 ± 6

[a] RSO membranes were treated with 2 mM NEM, 0.25 mM AmdiS, and 2 mM MTSET. Since mutant S333C was much more reactive, the duration of the treatment was reduced from 10 to 1 min. The indicated values give the residual uptake activity in RSO membranes as the percentage of that of an untreated sample. CSCSS is the control, and CXCSS represents I321C or S333C as indicated. The average and standard deviations of two to three independent measurements are reported.

the pretreated and untreated cells, suggesting that the cysteine residues were not accessible from the periplasmic side of the membrane for AmdiS (Figure 5C). As a positive control, cells expressing single-cysteine mutant S129C of the glutamate transporter GltT of *Bacillus stearothermophilus* were treated in the same way. The cysteine residue in S129C was shown to be in a periplasmic loop of the protein (*24*), and treatment of the cells with AmdiS under the same conditions prevented any further labeling with FM after the protein was purified (Figure 5C).

DISCUSSION

In this study, we investigated the folding of the loop between TMSs VIII and IX in the Na^+-dependent citrate transporter CitS of *K. pneumoniae* that was termed AH. Periodicity analysis revealed that the loop would have a strong amphipathic character when folded as an α-helix, a feature conserved throughout the 2HCT family even if the

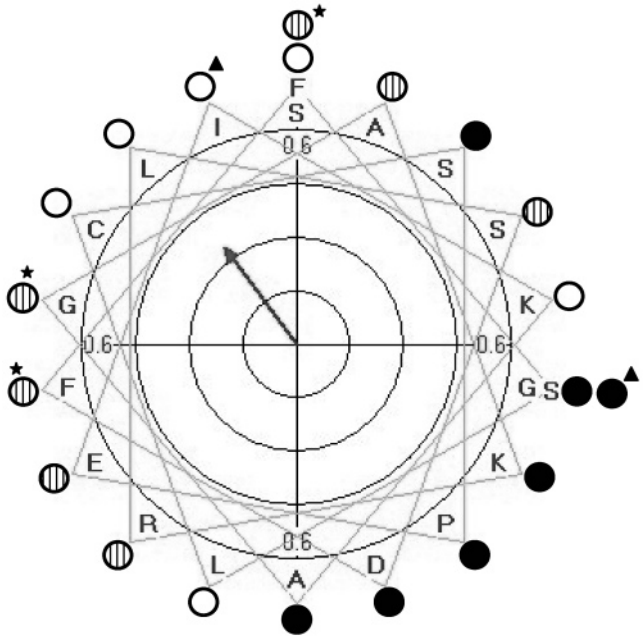

FIGURE 6: Helical wheel representation of the AH loop. Residues not accessible for FM and AmdiS were marked with empty circles, those with low accessibility with hatched circles, and those easily accessible with filled circles. The three categories were defined by having a significantly lower (empty), approximately equal (hatched), and significantly higher (solid) fluorescence intensity than protein staining intensity. Positions that after cysteine substitution resulted in transporters with less than 10% uptake activity are marked with an asterisk, and those that after labeling with NEM in RSO vesicles have decreased transport activity of less than 50% are marked with triangles.

amino acid sequence is not particularly well conserved. If so, the α-helix is likely to be a surface helix facing the membrane-embedded part of the transporter with the hydrophobic face and the water phase with the hydrophilic face. The experimental results are consistent with the loop forming

such an amphipathic surface helix. Figure 6 shows a helical wheel representation of the loop with the hydrophobic moment pointing at the hydrophobic face of the helix. Thus, cysteine residues at the positions of residues C317, L328, I321, and S314 residing at the hydrophobic face could not be labeled with fluorescein maleimide (FM), indicating that they are in close contact with other parts of the protein. At the opposite hydrophilic face, cysteine residues at the positions of residues A323, D330, P319, K326, G315, and S333 were easily labeled with FM, indicating that they are exposed to the water phase. Moreover, the latter positions that cover the complete loop were easily accessible for membrane impermeable AmdiS, but only when supplied at the cytoplasmic side of the membrane and not at the periplasmic side (Figure 5A,C), confirming that the whole stretch is cytoplasmic. Between the hydrophobic and hydrophilic faces of the helix, the accessibility of the cysteine residues is intermediate, suggesting that a large surface of the helix is embedded in the rest of the protein structure thereby restricting the accessibility pathway either in time or in space. The lack of labeling of cysteine residues at the positions of L316 and K322 at the hydrophilic side of the helix may be explained in this way. It was suggested previously that the AH loop would interact with C-terminal cytoplasmic loop Xa (*11*).

Replacement with cysteine resulted at only three positions, G324, F331, and F332 (Figure 6, asterisks), in transporter proteins with less than 10% activity, while at an additional two positions, I321 and S333 (Figure 6, triangles), modification of the cysteine residue resulted in significantly reduced activity. The less well-tolerated mutations are located at the more hydrophobic face of the helix and were only poorly accessible, suggesting a disturbed interaction with other parts of the protein. Moreover, G324 and F331, two residues in proximity, are actually quite well conserved in the AH loop throughout the 2HCT family (Figure 1D), emphasizing the importance of this side of the helix. Residue F332 is located next to residue I321 on the wheel. Treatment of the I321C mutant with NEM slowly resulted in the complete loss of activity of the transporter (Figure 4A). I321 is at the face of the helix that is not accessible for the fluorescent maleimide FM, and treatment with hydrophilic MTSET did not affect the activity (Table 1), indicating that only small hydrophobic molecules like NEM can access residue I321. Reaction of the cysteine residue at the position of residue S333 with NEM resulted in rapid but incomplete inactivation. S333 is the only residue of this group that is at the hydrophilic side of the helix and readily accessible from the water phase. It is the most C-terminal residue in the surface helix and may be close to catalytically active parts of neighboring loop Xa that forms part of the translocation site.

Cysteine mutants I321C and S333C were the only mutants in loop AH that were successfully inactivated by treatment with NEM in RSO membranes. Many other cysteine mutants, especially at the hydrophilic face of the helix, are likely to react with NEM, but apparently, the reaction did not result in reduced activity. The cysteine residues in the I321C and S333C mutants exhibited very different reactivities toward NEM (Figure 4A,B), a difference that was also observed for two endogenous cysteine residues in the Xa loop (*12*). C321 in AH, like C389 in Xa, reacted slowly with NEM, while C333 in AH, like C414 in Xa, reacted very fast. However, otherwise the behavior of the two pairs of cysteine residues was completely different. Both cysteine residues in the Xa loop are accessible from both sides of the membrane, and their reactivity is very sensitive to the catalytic state of the transporter. They were protected against reaction in the Na^+-bound state, and the reactivity is reduced in the citrate-bound state (*12*, *14*). In contrast, the two cysteine residues in the AH loop are only accessible from the cytoplasm, and their reactivity does not seem to be affected by the presence of co-ion and/or substrate at all. In fact, none of the cysteine mutants in the AH loop seems to react differently in the presence of Na^+ (Figure 3). It follows that the surface helix formed by loop AH does not sense the conformational changes of the protein during turnover and, therefore, most likely is not directly involved in substrate or co-ion binding and/or the translocation mechanism.

Amphipathic α-helices are commonly found in membrane proteins as transmembrane segments [class T helices in Eisenberg's classification (*25*, *26*)]. The hydrophobic side of the helix may face the phospholipid bilayer, while more polar residues at the opposite side are responsible for interactions with other transmembrane segments. More prominent are those transmembrane amphipathic helices in transport proteins that form a water-filled pore or channel that functions as the pathway for substrate and/or ion permeation. Examples of the latter have been described for the glutamate transporters GltT and human EAAT1 (*27*, *28*), human γ-aminobutyric acid (GABA) transporter GAT-1 (*29*), bacterial Na^+/proline transporter PutP (*30*), and the water channel aquaporin AQP1 (*31*). Little is known about the function of amphipathic helices formed by loop regions in transport proteins. Extracellular loop 4 of the rat serotonin transporter SERT was reported to form a helix−hinge−helix structure that could play a role in conformational changes but not in substrate binding (*32*), and in the rat type IIa Na^+/P_i transporter, part of extracellular loop 3 was proposed to form a 2.5-turn α-helical motif (*33*). The proline transporter ProP of *E. coli* was reported to contain an amphipathic α-helical structure in the C-terminal domain that is believed to play a role in osmosensing through interaction either with other membrane-associated proteins or with the surface of the membrane itself (*34*, *35*). In line with the properties of the AH loop reported here, it seems unlikely that amphipathic structures in loop regions of transport proteins play an important role in the transport mechanism itself.

Approximately one decade ago, in a study of the *E. coli* serine receptor Tsr, a short amphipathic sequence was identified that was shown to function as a determinant of membrane protein topology (*36*). Tsr is an integral membrane protein with two transmembrane segments connected by a large periplasmic domain and with a large cytoplasmic domain at the C-terminus. The 11-residue amphipathic sequence was located immediately downstream of the second transmembrane segment in the cytoplasmic domain. Deletion of the sequence or mutations that resulted in reduced amphipathicity resulted in increased mislocation of the C-terminal domain in the periplasm. As the amphipathic sequence was observed in most of the members of the family of chemoreceptors, it was concluded that the sequence was important for the proper insertion of this class of proteins into the membrane. Here, we propose a similar role for the amphipathic α-helix that is formed by loop AH in the CitS

protein. Evidence was presented showing that the helical hairpin formed by TMSs VIII and IX connected by the AH loop inserts into the membrane in a cooperative manner from the periplasmic side of the membrane (*16*, *18*). Before insertion, the TMS VIII−AH−TMS IX sequence would be translocated to the periplasm by the insertion machinery. Possible roles for the amphipathic helix formed by loop AH might be (i) stabilizing (part of) the segment after export in the periplasm, (ii) firmly positioning intermediate hydrophobic TMS IX in the membrane after insertion, and (iii) initiating insertion of the segment. In the latter case, the surface helix may resemble small antimicrobial peptides that fold as amphipathic helices and are known to bind at the membrane−water interface followed by insertion into the membrane [e.g., nisin (*37*)]. Further studies are needed to unravel the precise role of the amphipathic surface helix formed by loop AH in the biogenesis of this part of the CitS protein.

REFERENCES

1. Lolkema, J. S., and Slotboom, D. J. (2003) Classification of 29 families of secondary transport proteins into a single structural class using hydropathy profile analysis, *J. Mol. Biol. 327*, 901−909.
2. Bandell, M., Anasay, V., Rachidi, N., Dequin, S., and Lolkema, J. S. (1997) Membrane potential-generating malate (MleP) and citrate (CitP) transporters of lactic acid bacteria are homologous proteins. Substrate specificity of the 2-hydroxycarboxylate transporter family, *J. Biol. Chem. 272*, 18140−18146.
3. van der Rest, M. E., Molenaar, D., and Konings, W. N. (1992) Mechanism of Na(+)-dependent citrate transport in *Klebsiella pneumoniae*, *J. Bacteriol. 174*, 4893−4898.
4. Wei, Y., Guffanti, A. A., Ito, M., and Krulwich, T. A. (2000) *Bacillus subtilis* YqkI is a novel malic/Na^+-lactate antiporter that enhances growth on malate at low protonmotive force, *J. Biol. Chem. 275*, 30287−30292.
5. Krom, B. P., Aardema, R., and Lolkema, J. S. (2001) *Bacillus subtilis* YxkJ is a secondary transporter of the 2-hydroxycarboxylate transporter family that transports L-malate and citrate, *J. Bacteriol. 183*, 5862−5869.
6. Kawai, S., Suzuki, H., Yamamoto, K., and Kumagai, H. (1997) Characterization of the L-malate permease gene (maeP) of *Streptococcus bovis* ATCC 15352, *J. Bacteriol. 179*, 4056−4060.
7. Marty-Teysset, C., Lolkema, J. S., Schmitt, P., Diviès, C., and Konings, W. N. (1995) Membrane potential-generating transport of citrate and malate catalyzed by CitP of *Leuconostoc mesenteroides*, *J. Biol. Chem. 270*, 25370−25376.
8. Kastner, C. N., Schneider, K., Dimroth, P., and Pos, K. M. (2002) Characterization of the citrate/acetate antiporter CitW of *Klebsiella pneumoniae*, *Arch. Microbiol. 177*, 500−506.
9. van Geest, M., and Lolkema, J. S. (1996) Membrane topology of the sodium ion-dependent citrate carrier of *Klebsiella pneumoniae*. Evidence for a new structural class of secondary transporters, *J. Biol. Chem. 271*, 25582−25589.
10. van Geest, M., Nilsson, I., von Heijne, G., and Lolkema, J. S. (1999) Insertion of a bacterial secondary transport protein in the endoplasmic reticulum membrane, *J. Biol. Chem. 274*, 2816−2823.
11. van Geest, M., and Lolkema, J. S. (2000) Membrane topology of the Na^+/citrate transporter CitS of *Klebsiella pneumoniae* by insertion mutagenesis, *Biochim. Biophys. Acta 1466*, 328−338.
12. Sobczak, I., and Lolkema, J. S. (2004) Alternating access and a pore-loop structure in the Na^+-citrate transporter CitS of *Klebsiella pneumoniae*, *J. Biol. Chem. 279*, 31113−31120.
13. Krom, B. P., and Lolkema, J. S. (2003) Conserved residues R420 and Q428 in a cytoplasmic loop of the citrate/malate transporter CimH of *Bacillus subtilis* are accessible from the external face of the membrane, *Biochemistry 42*, 467−474.
14. Sobczak, I., and Lolkema, J. S. (2003) Accessibility of cysteine residues in a cytoplasmic loop of CitS of *Klebsiella pneumoniae* is controlled by the catalytic state of the transporter, *Biochemistry 42*, 9789−9796.
15. Bandell, M., and Lolkema, J. S. (2000) Arg-425 of the citrate transporter CitP is responsible for high affinity binding of di- and tricarboxylates, *J. Biol. Chem. 275*, 39130−39136.
16. van Geest, M., and Lolkema, J. S. (1999) Transmembrane segment (TMS) VIII of the Na^+/citrate transporter CitS requires downstream TMS IX for insertion in the *Escherichia coli* membrane, *J. Biol. Chem. 274*, 29705−29711.
17. Alder, N. N., and Johnson, A. E. (2004) Cotranslational membrane protein biogenesis at the endoplasmic reticulum, *J. Biol. Chem. 279*, 22787−22790.
18. van Geest, M., and Lolkema, J. S. (2000) Membrane topology and insertion of membrane proteins: Search for topogenic signals, *Microbiol. Mol. Biol. Rev. 64*, 13−33.
19. Gaillard, I., Slotboom, D. J., Knol, J., Lolkema, J. S., and Konings, W. N. (1996) Purification and reconstitution of the glutamate carrier GltT of the thermophilic bacterium *Bacillus stearothermophilus*, *Biochemistry 35*, 6150−6156.
20. Kaback, H. R. (1971) Bacterial Membranes, *Methods Enzymol. 22*, 99−120.
21. Konings, W. N., Barnes, E. N., Jr., and Kaback, H. R. (1971) Mechanisms of active transport in isolated membrane vesicles. 2. The coupling of reduced phenazine methosulfate to the concentrative uptake of β-galactosides and amino acids, *J. Biol. Chem. 246*, 5857−5861.
22. Kaplan, R. S., Mayor, J. A., Brauer, D., Kotaria, R., Walters, D. E., and Dean, A. M. (2000) The yeast mitochondrial citrate transport protein. Probing the secondary structure of transmembrane domain iv and identification of residues that likely comprise a portion of the citrate translocation pathway, *J. Biol. Chem. 275*, 12009−12016.
23. Karlin, A., and Akabas, M. H. (1998) Substituted-cysteine accessibility method, *Methods Enzymol. 293*, 123−145.
24. Slotboom, D. J., Sobczak, I., Konings, W. N., and Lolkema, J. S. (1999) A conserved serine-rich stretch in the glutamate transporter family forms a substrate-sensitive reentrant loop, *Proc. Natl. Acad. Sci. U.S.A. 96*, 14282−14287.
25. Eisenberg, D., Weiss, R. M., and Terwilliger, T. C. (1982) The helical hydrophobic moment: A measure of the amphiphilicity of a helix, *Nature 299*, 371−374.
26. Eisenberg, D., Schwarz, E., Komaromy, M., and Wall, R. (1984) Analysis of membrane and surface protein sequences with the hydrophobic moment plot, *J. Mol. Biol. 179*, 125−142.
27. Slotboom, D. J., Konings, W. N., and Lolkema, J. S. (2001) Cysteine-scanning mutagenesis reveals a highly amphipathic, pore-lining membrane-spanning helix in the glutamate transporter GltT, *J. Biol. Chem. 276*, 10775−10781.
28. Seal, R. P., and Amara, S. G. (1998) A reentrant loop domain in the glutamate carrier EAAT1 participates in substrate binding and translocation, *Neuron 21*, 1487−1498.
29. Zhou, Y., Bennett, E. R., and Kanner, B. I. (2004) The aqueous accessibility in the external half of transmembrane domain I of the GABA transporter GAT-1 is modulated by its ligands, *J. Biol. Chem. 279*, 13800−13808.
30. Pirch, T., Landmeier, S., and Jung, H. (2003) Transmembrane domain II of the Na^+/proline transporter PutP of *Escherichia coli* forms part of a conformationally flexible, cytoplasmic exposed aqueous cavity within the membrane, *J. Biol. Chem. 278*, 42942−42949.
31. Murata, K., Mitsuoka, K., Hirai, T., Walz, T., Agre, P., Heymann, J. B., Engel, A., and Fujiyoshi, Y. (2000) Structural determinants of water permeation through aquaporin-1, *Nature 407*, 599−605.
32. Mitchell, S. M., Lee, E., Garcia, M. L., and Stephan, M. M. (2004) Structure and function of extracellular loop 4 of the serotonin transporter as revealed by cysteine-scanning mutagenesis, *J. Biol. Chem. 279*, 24089−24099.
33. Lambert, G., Forster, I. C., Stange, G., Köhler, K., Biber, J., and Murer, H. (2001) Cysteine mutagenesis reveals novel structure−function features within the predicted third extracellular loop of the type IIa Na^+/P_i cotransporter, *J. Gen. Physiol. 117*, 533−546.
34. Culham, D. E., Tripet, B., Racher, K. I., Voegele, R. T., Hodges, R. S., and Wood, J. M. (2000) The role of the carboxyl terminal α-helical coiled-coil domain in osmosensing by transporter ProP of *Escherichia coli*, *J. Mol. Recognit. 13*, 309−322.
35. Zoetewey, D. L., Tripet, B. P., Kutateladze, T. G., Overduin, M. J., Wood, J. M., and Hodges, R. S. (2003) Solution structure of the C-terminal antiparallel coiled-coil domain from *Escherichia coli* osmosensor ProP, *J. Mol. Biol. 334*, 1063−1076.

36. Seligman, L., and Manoil, C. (1994) An amphipathic sequence determinant of membrane protein topology, *J. Biol. Chem. 269*, 19888−19896.

37. Breukink, E., and de Kruijff, B. (1999) The lantibiotic nisin, a special case or not? *Biochim. Biophys. Acta 1462*, 223−234.
BI047759Y